Human complement factor H Y402H polymorphism causes an age-related macular degeneration phenotype and lipoprotein dysregulation in mice

Michael Landowski[a], Una Kelly[a], Mikael Klingeborn[a], Marybeth Groelle[a], Jin-Dong Ding[a], Daniel Grigsby[a], and Catherine Bowes Rickman[a,b,1]

[a]Department of Ophthalmology, Duke Eye Center, Duke University, Durham, NC 27710; and [b]Department of Cell Biology, Duke University, Durham, NC 27710

Edited by Jeremy Nathans, The Johns Hopkins University, Baltimore, MD, and approved January 11, 2019 (received for review August 14, 2018)

One of the strongest susceptibility genes for age-related macular degeneration (AMD) is complement factor H (*CFH*); however, its impact on AMD pathobiology remains unresolved. Here, the effect of the principal AMD-risk–associated CFH variant (Y402H) on the development and progression of age-dependent AMD-like pathologies was determined in vivo. Transgenic mice expressing equal amounts of the full-length normal human CFH Y402 (*CFH-Y/0*) or the AMD-risk associated CFH H402 (*CFH-H/H*) variant on a *Cfh*$^{-/-}$ background were aged to 90 weeks and switched from normal diet (ND) to a high fat, cholesterol-enriched (HFC) diet for 8 weeks. The resulting phenotype was compared with age-matched controls maintained on ND. Remarkably, an AMD-like phenotype consisting of vision loss, increased retinal pigmented epithelium (RPE) stress, and increased basal laminar deposits was detected only in aged *CFH-H/H* mice following the HFC diet. These changes were not observed in aged *CFH-Y/0* mice or in younger (36- to 40-week-old) *CFH* mice of both genotypes fed either diet. Biochemical analyses of aged *CFH* mice after HFC diet revealed genotype-dependent changes in plasma and eyecup lipoproteins, but not complement activation, which correlated with the AMD-like phenotype in old *CFH-H/H* mice. Specifically, apolipoproteins B48 and A1 are elevated in the RPE/choroid of the aged *CFH-H/H* mice compared with age-matched control *CFH-Y/0* fed a HFC diet. Hence, we demonstrate a functional consequence of the Y402H polymorphism in vivo, which promotes AMD-like pathology development and affects lipoprotein levels in aged mice. These findings support targeting lipoproteins as a viable therapeutic strategy for treating AMD.

age-related macular degeneration | complement | lipoproteins | RPE | genetic risk

Age-related macular degeneration (AMD) is the leading cause of irreversible central blindness in elderly populations of industrialized nations (1). Risk for AMD is conferred predominantly by advanced aging and is modulated by genetic risk factors and environmental stresses (2–4). Notably, variants in complement system proteins are strongly associated with risk for AMD development and progression (5–13). Complement is a critical component of innate immunity responsible for the opsonization and removal of bacterial and apoptotic cell debris, as well as recruitment of immune cells to sites of infection and tissue damage (14, 15). The role of complement in AMD pathogenesis remains unclear as highlighted by the recent phase III clinical trial failure of lampalizumab, a factor D inhibitor that blocks activation of the alternative complement pathway. Lampalizumab had no effect in reducing growth of geographic atrophy lesions in patients with late dry AMD, despite promising phase II clinical trial results (16). Understanding the role of complement in AMD will undoubtedly lead to important insights for novel therapeutic strategies for AMD.

One of the most published and replicated genetic variants associated with AMD risk is the tyrosine (Y) to histidine (H) substitution at amino acid 402 (Y402H) in complement factor H (CFH for the human protein, Cfh for the mouse protein) (6–9). CFH is the soluble regulator of the alternative complement pathway and prevents formation of its C3 convertase by acting as a cofactor for factor I-mediated proteolytic inactivation of C3b (17) and as a decay accelerator that prevents binding of factor B (FB) to C3b (18). The Y402H amino acid lies outside of the complement-regulating short consensus repeats (SCRs) 1–4 of CFH, and thus it is not surprising that no differences in regulation of fluid phase complement activation between the Y402 and H402 variants have been detected (19–22). Instead, the Y402H polymorphism is located in SCR 7, a region that is known to mediate CFH binding to polyanions, such as heparin, glycosaminoglycans, and C-reactive protein (CRP) (23, 24). The Y402H polymorphism has been shown to decrease the binding of CFH to heparin (21, 25), M6 protein of *Streptococcus pyogenes* (25, 26), CRP (21, 25–27), Bruch's membrane (BrM) (28), malondialdehyde (MDA) epitopes (29), and oxidized phospholipids (30). The significance of these variant differences in predisposing an aging eye to AMD progression can be gleaned from the study of aged hemizygous ($^{+/-}$) and knockout ($^{-/-}$) murine *Cfh* mice exposed to an environmental stress (31). Aged *Cfh*$^{+/-}$ mice fed an 8-wk high fat, cholesterol-enriched (HFC) diet develop AMD-like pathologies, including rod-mediated visual dysfunction, increased numbers of multinucleate retinal pigmented

Significance

The complement factor H (CFH) Y402H polymorphism (rs1061170) imparts the strongest risk for age-related macular degeneration (AMD), the leading cause of blindness in the elderly. Popular thinking holds that the CFH H402 variant increases complement activation in the eye, predisposing susceptibility to disease. However, clinical trials of complement inhibitors in AMD patients have failed. Here we provide an explanation, showing CFH variant-specific differences in the presentation of AMD-like pathologies. We show that aged mice expressing the human H402, but not Y402 variant, (*i*) develop AMD-like symptoms and (*ii*) display differences in their systemic and ocular lipoprotein levels, but not in their complement activation, after diet. These findings support targeting lipoproteins for the treatment of AMD.

Author contributions: M.L., U.K., and C.B.R. designed research; M.L., U.K., M.K., M.G., J.-D.D., and D.G. performed research; M.L., U.K., M.K., J.-D.D., D.G., and C.B.R. analyzed data; and M.L., U.K., M.K., and C.B.R. wrote the paper.

The authors declare no conflict of interest.

This article is a PNAS Direct Submission.

[1]To whom correspondence should be addressed. Email: bowes007@duke.edu.

This article contains supporting information online at www.pnas.org/lookup/suppl/doi:10.1073/pnas.1814014116/-/DCSupplemental.

Published online February 11, 2019.

epithelium (RPE) cells, and increased basal laminar deposits (BLamDs) while, paradoxically, aged $Cfh^{-/-}$ mice only develop increased BLamDs following HFC diet consumption (31). A major difference between $Cfh^{+/-}$ and $Cfh^{-/-}$ mice is the absence of a circulating reservoir of complement proteins in $Cfh^{-/-}$ mice due to the lack of Cfh (31, 32). This study demonstrates that the role of the H402 CFH variant in AMD pathogenesis may lie at the interplay between complement and consumption of a HFC diet in aged mice (31, 33).

In the present study we test the hypothesis that the H402 polymorphism contributes to the development of AMD-like pathologies in mice stressed with AMD-relevant chronic insults. We show aged mice expressing the H402 CFH risk variant (*CFH-H/H*) developed AMD-like pathologies compared with age-matched mice expressing the Y402 CFH variant (*CFH-Y/0*) after an 8-wk HFC diet regime. Analysis of the plasmas and eyecups from aged *CFH* mice on and off HFC diet revealed that levels of complement activation proteins were similar for both genotypes and suggested the phenotypic differences between these mice is not solely due to complement activation but another consequence of the HFC diet. One effect of the HFC diet is to augment plasma chylomicrons (CMs), very low-density lipoproteins (VLDLs), and low-density lipoproteins (LDLs) in mice that are normally present at low concentrations and critical for delivering cholesterol to peripheral tissues (34). However, risk for developing AMD is not associated with increased levels of plasma CMs, VLDLs, or LDLs, but rather high-density lipoproteins (HDLs) (35–39). This is in stark contrast to atherosclerosis where risk is strongly conferred by increased plasma LDL but not variants in CFH (40, 41). The effects of the HFC diet on lipoproteins in aged *CFH* mice was examined, revealing an increase in plasma LDL containing ApoB100 and ApoE that was not as great in the *CFH-H/H* mice compared with the *CFH-Y/0* mice. Intriguingly, in the eyecup lysates we observed increases in ApoB48 and ApoA1 only in aged *CFH-H/H* mice after the HFC diet. These results show that the CFH Y402H polymorphism impacts HFC diet-induced AMD-like pathologies and lipoprotein levels in vivo. These findings suggest there is an intersection between complement and lipid homeostasis that may explain mechanistic differences between AMD and atherosclerosis and support targeting lipoproteins as viable therapeutic targets for AMD.

Results

Fluid Phase Complement Proteins in Human *CFH* Transgenic Mice. We have previously described the transgenic mouse lines expressing full-length human CFH on a $Cfh^{-/-}$ background that were created to study the Y402H polymorphism in vivo (42). Human CFH expressed by these hemizygous *CFH:*$Cfh^{-/-}$ mice (referred to as *CFH* mice, as all of the lines expressing human CFH are on a *Cfh*-null C57BL/6J background) regulates activation of the mouse alternative complement pathway and rescues the kidney from damage seen in $Cfh^{-/-}$ mice, effectively replacing the mouse Cfh, which is absent in these mice (32, 42). We also showed that there is twofold more CFH protein in *CFH-Y/0* plasma (~20 μg/mL) than in *CFH-H/0* plasma (~10 μg/mL). Hemizygous *CFH-H/0* were bred together to generate homozygous *CFH-H/H* mice to correct this problem (42). Concentrations of plasma CFH (*SI Appendix*, Fig. S1*A*), C3 (*SI Appendix*, Fig. S1*B*), and FB (*SI Appendix*, Fig. S1*C*) are the same in homozygous *CFH-H/H* mice compared with hemizygous *CFH-Y/0* mice, and as much as twice the concentrations of the levels detected in hemizygous *CFH-H/0* mice.

In addition to systemic sources, CFH is locally produced and secreted by ocular tissues, such as the RPE and choroidal endothelial cells (43). We evaluated the expression and concentration of CFH and C3 in the eyecup (RPE/BrM/choroid/sclera) of *CFH* mice (*SI Appendix*, Fig. S2). Hemizygous *CFH-Y/0* mice and homozygous *CFH-H/H* mice express similar levels of *CFH* transcript in the eyecup. In contrast, the *CFH* transcript levels are about half in the hemizygous *CFH-H/0* compared with the *CFH-Y/*0 and *CFH-H/H* and absent in $Cfh^{-/-}$ mouse eyecups (*SI Appendix*, Fig. S2*A*). *C3* mRNA eyecup expression is equivalent in all these genotypes (*SI Appendix*, Fig. S2*B*). Protein CFH concentrations in the eyecup followed the *CFH* mRNA expression pattern (*SI Appendix*, Fig. S2*C*). Because CFH regulates the level of C3 and its cleavage products, C3b and iC3b, we measured these protein amounts as an indication for the level of functional CFH in the eyecup. Levels of C3/C3b/iC3b correlate with CFH protein levels (*SI Appendix*, Fig. S2*D*).

In the present study the cumulative effects of aging and consumption of an 8-wk HFC diet were only tested in hemizygous *CFH-Y/0* and homozygous *CFH-H/H* mice because these mouse lines express and secrete equal amounts of the human normal and AMD-risk–associated CFH variants, respectively, both systemically in the circulation and locally in the eyecup.

Visual Function Decline Associates with Human H402 CFH, Aging, and HFC Diet. Advanced aging and consumption of an HFC diet is sufficient to cause vision loss, RPE stress, and BLamD accumulation in specific genotypes of mice (31, 44, 45). We tested whether the Y402H polymorphism influences the development of an AMD-like phenotype in the *CFH* mice when combined with these risk factors. *CFH-Y/0* and *CFH-H/H* mice were aged to at least 90 wk and maintained on a normal rodent diet (ND) or switched to an HFC diet for 8 wk. Scotopic electroretinography (ERG) was used to measure visual function in the aged *CFH* mice following the HFC diet, as rod photoreceptor dysfunction is an early sign of AMD (46) and diminished scotopic ERG B-wave responses have been shown in other AMD mouse models following an HFC diet (31, 44, 47). In contrast to all of the other mouse groups tested here, only aged *CFH-H/H* mice fed an HFC diet (*CFH-H/H*~HFC) developed significant decreases in their ERG B-wave amplitudes compared with age-matched *CFH-H/H* mice fed an ND (*CFH-H/H*~ND) (Fig. 1*A*). There were no differences in the ERG B-wave amplitudes between the aged *CFH-Y/0* mice continued on an ND (*CFH-Y/0*~ND) compared with age-matched *CFH-Y/0* mice fed an HFC diet (*CFH-Y/0*~HFC) or in *CFH-H/H*~ND mice (Fig. 1*A*). Visual function in younger adult (36- to 40-wk-old) *CFH* mice of either genotype fed an ND or switched to an HFC diet was not changed (*SI Appendix*, Fig. S3). Together, these findings establish an age-dependent effect of the CFH H402 risk variant on scotopic B-wave responses following consumption of an HFC diet in mice.

Scotopic ERG A-wave responses were analyzed to assess photoreceptor activity. There was a trend toward lower A-wave amplitudes in aged *CFH-H/H*~HFC compared with all three other groups, but this did not reach statistical significance (*SI Appendix*, Fig. S4*A*). Bmax1 and Bmax2 values representing rod-dominant and cone-dominant responses, respectively, were calculated. Significant decreases ($P < 0.05$) were observed in the rod-dominant Bmax1 responses (*SI Appendix*, Fig. S4*B*)—but not in the cone-dominant Bmax2 responses (*SI Appendix*, Fig. S4*C*)—of aged *CFH-H/H*~HFC mice compared with aged *CFH-H/H*~ND mice. There was no change in Bmax1 (*SI Appendix*, Fig. S4*B*) or Bmax2 (*SI Appendix*, Fig. S4*C*) values in aged *CFH-Y/0*~ND and ~HFC mice. These results indicate the CFH H402 variant modulates rod-dominant visual activity following the HFC diet treatment.

RPE Stress Increases in Mice Expressing Human H402 CFH with Age and HFC Diet. In this study RPE stress was assessed as the degree of RPE dysmorphia and quantitated by the number of multinucleate RPE cells with three or more nuclei. Multinucleate RPE cells are associated with AMD (44), AMD mouse models (31, 44, 47), and normal aging in mice (48). RPE flat mounts were labeled

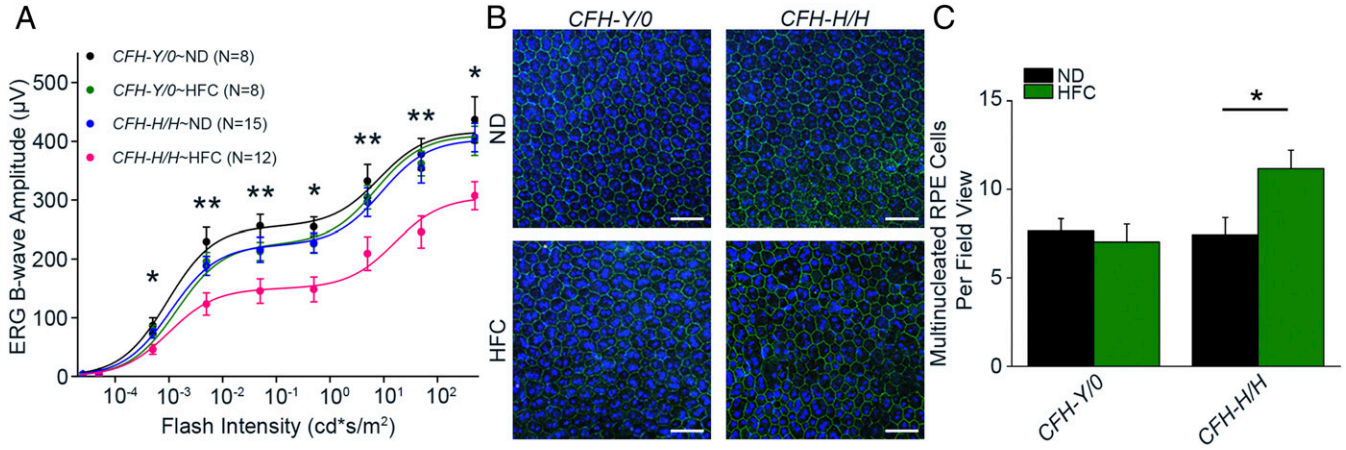

Fig. 1. AMD-like changes including decreased visual function and increased RPE stress occurs only in aged *CFH-H/H*~HFC mice. (*A*) Scotopic ERG flash responses in aged (90+ wk) *CFH* mice fed an ND or HFC diet. Visual function was assessed by scotopic ERG and presented as fitted lines of the B-wave amplitude averages using the equation $R = (Bmax1 \times I/I + I1)/(Bmax2 \times I/I + I2)$. No differences in the scotopic ERG B-wave responses were observed between aged *CFH-Y/0*~ND (black), *CFH-Y/0*~HFC (green) mice, and *CFH-H/H*~HFC (blue). Only aged *CFH-H/H*~HFC mice (pink) develop significant attenuated ERG B-wave responses compared with aged *CFH-H/H*~ND mice. $*P < 0.05$ and $**P < 0.01$ post hoc Tukey, following a significant genotype by diet interaction by ANOVA for the B-wave amplitudes. (*B*) RPE stress as ascertained by RPE dysmorphia in aged *CFH* mice following HFC diet. Representative confocal fluorescence images (40× magnification) of RPE flat mounts near the optic nerve stained with Hoechst 33342 (blue, nuclei) and anti–ZO-1 (green) from aged *CFH* mice on ND and HFC diet. RPE dysmorphia in aged *CFH* mice was measured by the number of multinucleate ($n \geq 3$ nuclei) RPE cells within each image. There are more multinucleate RPE cells in aged *CFH-H/H*~HFC mice. (Scale bars, 50 μm.) (*C*) Quantitation of multinucleate ($n \geq 3$ nuclei) RPE cells per field view in aged *CFH* mice on ND and HFC diet shows no change in the number of multinucleate RPE cells in aged *CFH-Y/0*~ND ($n = 8$) and *CFH-Y/0*~HFC ($n = 8$) mice. Aged *CFH-H/H*~HFC mice ($n = 11$) have a statistically larger number of multinucleate cells per field view than *CFH-H/H*~ND mice ($n = 7$). $*P < 0.05$ post hoc Tukey following a significant genotype by diet interaction by ANOVA for the mean number of multinucleate RPE cells. Data are presented as mean ± SEM.

with an antibody against the tight junction-associated protein zonula occludens 1 (ZO-1) and stained with Hoescht 33258 to visualize RPE cell membranes and nuclei, respectively (Fig. 1*B*). No change in the number of multinucleate RPE cells was detected in aged *CFH-Y/0*~ND and ~HFC mice (Fig. 1*C*). There was, however, a significant ($P < 0.05$) increase in the number of multinucleate RPE cells in aged *CFH-H/H*~HFC mice compared with aged *CFH-H/H*~ND mice (Fig. 1*C*). In younger adult *CFH*~ ND and ~HFC mice, fewer numbers of multinucleate RPE cells were detected overall and there was no significant effect of diet on the RPE in either genotype (*SI Appendix*, Fig. S5). These data demonstrate an age-dependent CFH variant difference contributing to RPE stress in the old *CFH-H/H* mice after 8 wk of HFC diet.

HFC Diet-Induced BLamD Accumulation Increase in Mice Expressing Human H402 CFH. BLamDs have been shown to accumulate in mouse models of AMD, although these deposits are histopathologically different from those detected in human AMD (31, 42, 47, 49). However, deposits can also occur in the absence of other AMD-like changes, like visual impairment or RPE stress, as we have shown in aged $Cfh^{-/-}$ mice following HFC diet that do not develop decreased ERG B-wave responses or increased numbers of multinucleate RPE cells compared with age-matched $Cfh^{+/-}$ mice after HFC diet (31). In the present study, deposit accumulation was quantitatively measured in aged *CFH* mice on and off HFC diet by transmission electron microscopy (TEM), as previously described (31, 42).

All aged *CFH* mice irrespective of diet treatment had BLamDs (Fig. 2*A*). The deposit heights were graphed by their cumulative frequencies enabling the qualitative assessment of the deposit size distribution within each genotype and diet. Furthermore, deposit height averages were calculated for each mouse to allow for statistical comparisons. No change in BLamD sizes was noted between aged *CFH-Y/0*~ND and ~HFC mice (Fig. 2 *B* and *D*). Aged *CFH-H/H*~ND mice accumulate significantly ($P < 0.05$) less deposits than age-matched *CFH-Y/0*~ND mice (Fig. 2 *C* and *D*). Only aged *CFH-H/H* mice develop significantly ($P < 0.05$) larger deposits when fed an HFC diet compared with those maintained on ND (Fig. 2 *C* and *D*). BLamD accumulation was also analyzed in younger adult (36- to 40-wk-old) *CFH* mice of both genotypes and on both diets to confirm that advanced aging is required for HFC-induced deposit formation. As expected, there was no accumulation of BLamDs in young *CFH* mice fed either diet (*SI Appendix*, Fig. S6). These results establish a CFH variant difference in advanced age-related and HFC diet-induced deposits.

HFC Diet-Induced Complement Activation Is Independent of CFH 402 Variant Expressed. The levels of complement components were compared in plasma and eyecups of aged *CFH-Y/0*~HFC and *CFH-H/H*~HFC mice to measure complement activation in response to the HFC diet. There were significant ($P < 0.05$) increases in plasma levels of CFH (Fig. 3*A*), FB (Fig. 3*B*), and C3/C3b/iC3b (Fig. 3*C*) in both aged *CFH-Y/0* and *CFH-H/H* mice following the HFC diet compared with ND-fed age-matched controls. Further support for increased complement activation in the plasma was shown by analysis of levels of iC3b, a C3 fragment indicative of complement activation, in reduced plasma samples obtained from aged *CFH* ND and HFC diet-fed mice (Fig. 3*D*). There was a significant increase of plasma iC3b in both *CFH-Y/0*~HFC ($P < 0.01$) and *CFH-H/H*~HFC diet mice ($P < 0.05$) compared with ND-fed controls (Fig. 3*D*). No significant differences in the levels of plasma iC3b were measured between aged *CFH-Y/0*~HFC and *CFH-H/H*~HFC mice (Fig. 3*D*).

Complement activation in eyecup (RPE/BrM/choroid/sclera) lysates of aged *CFH-Y/0*~HFC and *CFH-H/H*~HFC mice was assessed by measuring total FB and C3/C3b/iC3b. There was a significant increase in FB levels in the eyecups of both aged *CFH-Y/0* ($P < 0.01$) and *CFH-H/H* ($P < 0.05$) mice on HFC diet compared with ND-fed controls, but this increase in FB with HFC diet was not different between the genotypes (Fig. 3*E*). Eyecup levels of C3/C3b/iC3b in either genotype was unchanged following consumption of the HFC diet (Fig. 3*F*). These results

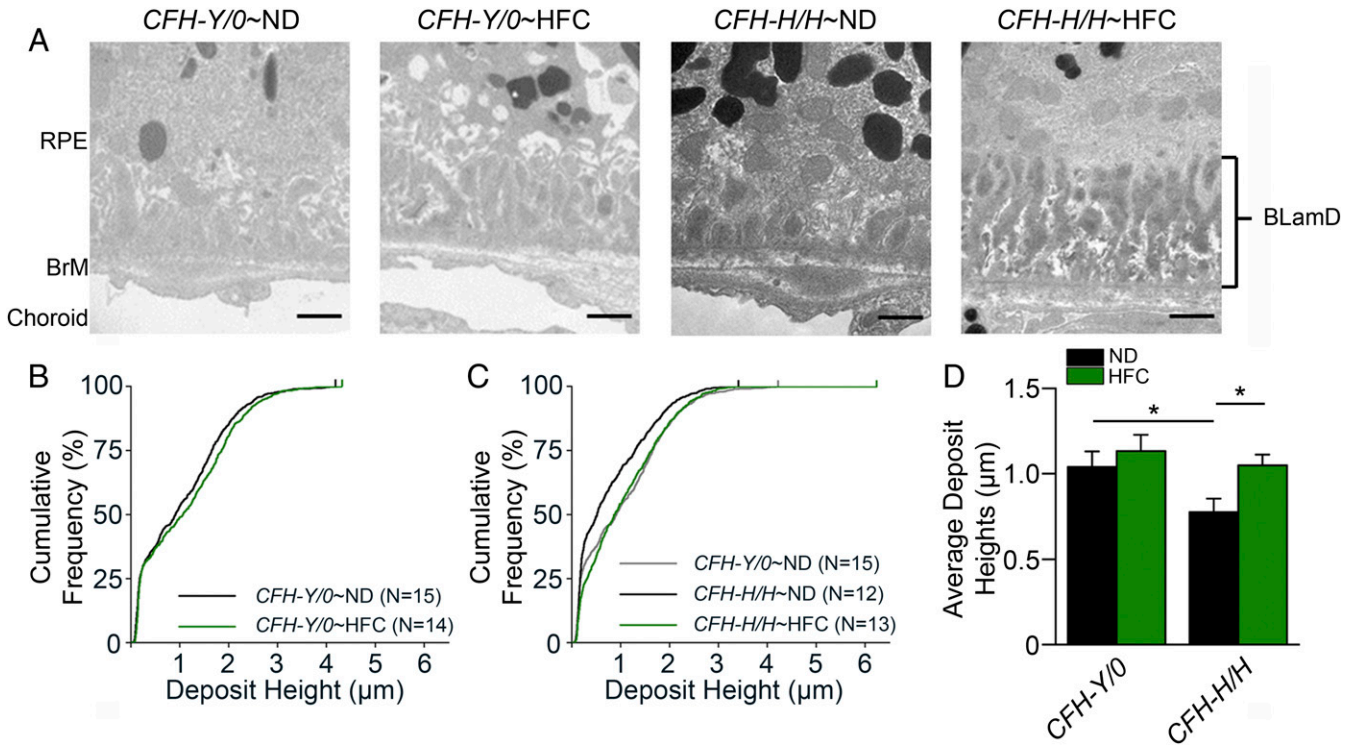

Fig. 2. Aged *CFH-H/H*~HFC mice have increased BLamDs. (*A*) TEM images (15,000× magnification) of the region were used to quantitate the size of BLamDs in aged *CFH-Y/0* and *CFH-H/H* mice on ND and HFC diet. Representative TEM images show that all aged *CFH-Y/0* and *CFH-H/H* mice have BLamDs irrespective of diet treatment. However, deposits in aged *CFH-H/H*~ND mice appear the smallest compared with the other groups in this study. (Scale bars, 1 μm.) (*B*) BLamD heights in aged *CFH-Y/0*~ND and ~HFC mice. BLamD heights were measured from the elastic layer of BrM to the top of the largest deposit within each TEM image. Cumulative frequencies of the BLamD heights were plotted against deposit height to illustrate the distribution of deposit heights for the genotype and diet. There is a slight shift to the right in the distribution of larger deposits and demonstrates an increase in deposit sizes in aged *CFH-Y/0*~HFC mice (green) compared with aged *CFH-Y/0*~ND mice (black). (*C*) Deposit heights in aged *CFH-H/H*~ND and *CFH-H/H*~HFC mice. Aged *CFH-Y/0*~ND mice (gray) have larger deposits compared with aged *CFH-H/H*~ND mice (black) but have similar deposits as those found in aged *CFH-Y/0*~ND mice. (*D*) Averages of deposit heights in aged *CFH* mice after HFC diet. The deposit height averages replicate the trends observed in the cumulative frequency plots. **P* < 0.05 post hoc Tukey following a significant genotype by diet interaction by ANOVA for the mean BLamD heights. Data are presented as mean ± SEM.

suggest that the phenotypic differences between aged *CFH-Y/0*~HFC and *CFH-H/H*~HFC mice is not solely due to HFC-induced complement activation.

HFC Diet-Induced Plasma LDL Levels Are CFH Variant Dependent. Consumption of a HFC diet increases circulating cholesterol and lipoproteins in wild-type C57BL/6J mice (34). Total plasma cholesterol levels were analyzed to test for differences in HFC-diet–induced cholesterol increases between aged *CFH* mice. Significantly higher levels of plasma cholesterol were found in both aged *CFH-Y/0*~HFC ($P < 0.001$) and *CFH-H/H*~HFC ($P < 0.001$) mice compared with ND-fed controls (Fig. 4*A*). Interestingly, aged *CFH-H/H*~HFC mice had significantly lower ($P < 0.01$) total plasma cholesterol than aged *CFH-Y/0*~HFC mice (Fig. 4*A*). Plasmas obtained from aged *CFH*~ND and ~HFC diet mice were fractionated by fast protein liquid chromatography (FPLC) to determine the distribution of cholesterol within CM/VLDL, LDL, and HDL particles. In *CFH*~ND mice, the plasma cholesterol is primarily contained within HDLs (*SI Appendix*, Fig. S7). Following consumption of the HFC diet in these mice, cholesterol is also detected within CM/VLDL and LDL particles (Fig. 4*B*). Cholesterol levels in the FPLC fractions corresponding to LDLs are significantly lower ($P < 0.05$) in aged *CFH-H/H*~HFC mice compared with *CFH-Y/0*~HFC mice (Fig. 4 *B* and *C*).

Apolipoprotein concentrations were measured by Western blot analysis of fasted plasma samples to confirm the FPLC results. ApoB100 and ApoB48 (*SI Appendix*, Fig. S8), as well as ApoE (*SI Appendix*, Fig. S8), are predominantly found in the fractions that correlate with CMs, VLDLs, and LDLs in both *CFH-Y/0*~HFC and *CFH-H/H*~HFC mice. In contrast, ApoA1 is only detected in the HDL fractions in all genotypes regardless of diet (*SI Appendix*, Fig. S8). There was significantly higher ($P < 0.001$) plasma ApoB48 levels in both aged *CFH-Y/0*~HFC and *CFH-H/H*~HFC mice compared with ND-fed controls but the levels were the same in both genotypes after diet treatment (Fig. 4*D*). ApoB100 was significantly higher ($P < 0.05$) in aged *CFH-Y/0*~HFC mice compared with aged *CFH-Y/0*~ND and *CFH-H/H*~HFC mice (Fig. 4*E*). Significantly higher levels of plasma ApoE were observed in *CFH-Y/0*~HFC ($P < 0.001$) and *CFH-H/H*~HFC ($P < 0.01$) mice compared with ND controls, and these levels were significantly higher ($P < 0.05$) in aged *CFH-Y/0*~HFC mice compared with aged *CFH-H/H*~HFC mice (Fig. 4*F*). No differences in plasma ApoA1 levels were measured in aged *CFH* mice with either diet treatment (Fig. 4*G*). Taken together, these results establish that the CFH Y402H polymorphism impacts levels of plasma VLDLs and LDLs containing both ApoB100 and ApoE.

Eyecup Apolipoprotein Levels Increase in *CFH-H/H* Mice Fed HFC Diet. CFH can compete with ApoB100- and ApoE-containing lipoproteins for their binding to BrM ex vivo (31). The apolipoprotein content in eyecups of aged *CFH* mice on and off an HFC diet were analyzed by Western blot to test whether the H402 polymorphism impacts lipoprotein retention in aged murine BrM. There was a significant increase in the eyecup levels of

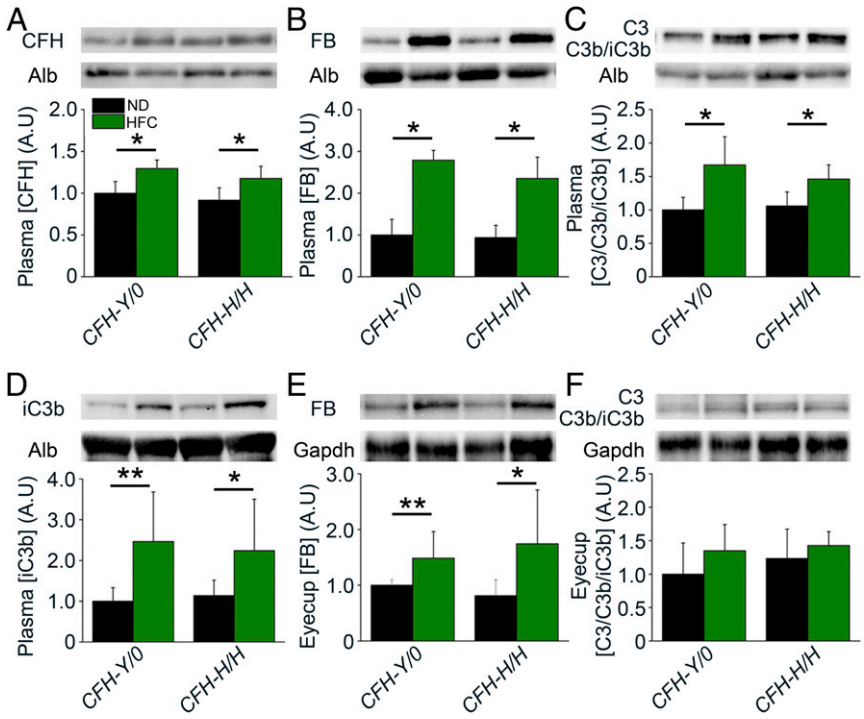

Fig. 3. HFC diet-induced complement activation is *CFH* variant independent. (*A–D*) Densitometric analysis of CFH (*A*), FB (*B*), C3/C3b/iC3b (*C*), and iC3b (*D*) immunoblots of plasmas from aged *CFH*~ND and ~HFC mice after fasting. Plasma CFH, FB, and C3/C3b/iC3b significantly increased in fasted *CFH-Y/0*~HFC and *CFH-H/H*~HFC mice compared with ND-fed controls but were no differences in the levels between the genotypes after HFC diet treatment ($n = 4$). (*D*) Plasma samples were reduced before loading to quantitate iC3b levels ($n = 8$). Both *CFH-Y/0*~HFC and *CFH-H/H*~HFC mice had significantly increased levels of plasma iC3b compared with ND fed controls and show similar levels of plasma complement activation between these genotypes after HFC diet. (*E* and *F*) Densitometric analysis of FB (*E*) and C3/C3b/iC3b (*F*) immunoblots of eyecups (RPE/BrM/choroid/sclera) from fasted, aged *CFH*~ND and ~HFC mice ($n = 7$). FB levels were significantly higher in fasted *CFH-Y/0*~HFC and *CFH-H/H*~HFC mice compared with ND fed controls but not different between the genotypes on an HFC diet. Interestingly, no statistically significant differences in the C3/C3b/iC3b levels were detected between the genotypes on ND versus HFC diet ($n = 7$). $^{*}P < 0.05$ and $^{**}P < 0.01$ post hoc Tukey following a significant genotype by diet interaction by ANOVA for the densitometric arbitrary units. Data are presented as mean ± SD.

ApoB48 (Fig. 5*A*) ($P < 0.01$) and ApoA1 (Fig. 5*D*) ($P < 0.05$) found only in aged *CFH-H/H* mice following the HFC diet compared with levels of ApoB100 (Fig. 5*B*) or ApoE (Fig. 5*C*), which were unchanged in either genotype following the HFC diet. This result supports a CFH H402 risk variant specific role in increasing ApoB48 and ApoA1 levels in the eyecup in response to advanced age and the HFC diet.

Discussion

AMD is a complex retinal degeneration presenting in the elderly with limited therapeutic options for affected patients. One of the strongest genetic risk factors for AMD is the *CFH* Y402H polymorphism, but the role of the H402 CFH variant in AMD is unknown (6–9). We addressed this problem through the generation of transgenic mice expressing equal concentrations of the full-length normal human CFH Y402 versus the AMD-risk associated CFH H402 variant on a *Cfh*-null background (*CFH-Y/0* and *CFH-H/H*, respectively). We analyzed the contribution of these genotypes to causing an AMD phenotype by testing their effects in the presence of additional known AMD risk factors, advanced age and a Western-style diet. *CFH* mice were aged to 90 wk and maintained on an ND or switched to an HFC diet for 8 wk to elicit AMD-like pathologies as observed in other mouse models (31, 44, 45, 47). An AMD-like phenotype consisting of decreased ERGs, increased RPE multinucleate cells, and increased BLamDs was observed only in the aged *CFH-H/H* mice fed an HFC diet compared with age-matched control *CFH-H/H* mice maintained on an ND, age-matched *CFH-Y/0* mice fed either diet and young adult *CFH* mice fed either diet. While we are not the first laboratory to use mice to investigate the role of the H402 variant in AMD (50–52), our study identifies CFH variant differences in a chronic, multifactorial model expressing the full-length human CFH variants and incorporating advanced aging and environmental stress.

The risk association between the *CFH* Y402H polymorphism and AMD is widely considered to result from reduced activity of the CFH H402 variant in regulation of C3 activation resulting in excess complement-mediated inflammation and tissue damage in posterior eye tissues (53). Previous studies have shown increased activated complement components in the plasmas of AMD patients (54–57) and localization of activated complement products within drusen of AMD donor eyes (58–60). However, recent clinical trial failures of complement inhibitors for AMD have been unsuccessful, which may be due to our incomplete understanding of the role of activated complement components in AMD development (61). In the present study, complement activation levels were the same in both *CFH* genotypes, whereas visual loss and RPE stress is detected only in the *CFH-H/H~HFC* mice. These phenotypic differences most likely reflect the H402 polymorphism impairing a complement-independent function of CFH, such as binding to a biological molecule or epitope, as has been described in previous studies (21, 25–30, 52). For example, there is differential binding to heparan sulfate (28), which may result in less CFH H402 binding to the ECM or cell surfaces. In addition, differential binding of Y402 and H402 variants to CD47 results in the H402 variant inhibiting binding of thrombospondin-1 to CD47 on mononuclear phagocytes, thus preventing their subsequent elimination (52). Finally, differential binding to MDA has been shown in which the Y402 variant has a higher affinity for MDA, thereby neutralizing

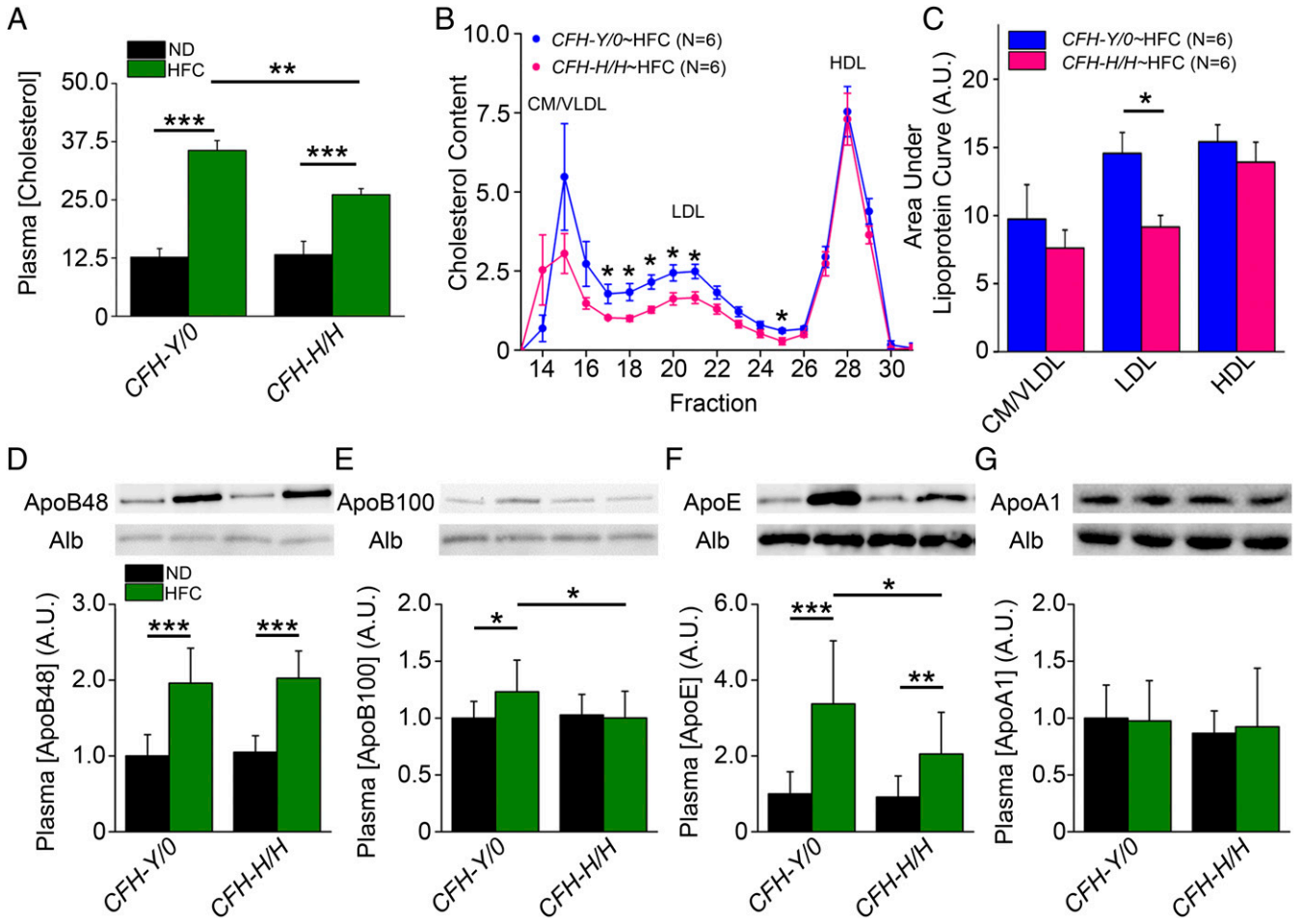

Fig. 4. Plasma lipoprotein levels are *CFH* variant dependent. (*A*) Total plasma cholesterol from fasted, aged *CFH*~ND and ~HFC mice. Both aged *CFH-Y/0*~HFC ($n = 11$) and *CFH-H/H*~HFC ($n = 11$) mice have statistically significant higher plasma cholesterol than age-matched *CFH-Y/0*~ND ($n = 8$) and *CFH-H/H*~HFC ($n = 8$) mice, respectively. Aged *CFH-H/H*~HFC mice have statistically lower plasma cholesterol compared with aged *CFH-Y/0*~HFC mice. (*B* and *C*) FPLC fractionation of plasma from fasted *CFH*~HFC mice. (*B*) Following the HFC diet, cholesterol was detected in fractions corresponding to CMs/ VLDLs, LDLs, and HDLs. LDL fractions 17–21 and 25 were statistically higher in aged *CFH-Y/0*~HFC mice (blue) compared with aged *CFH-H/H*~HFC mice (pink). (*C*) The area under the fractionated lipoprotein curve were calculated for each lipoprotein class and confirmed higher plasma LDL levels in aged *CFH-Y/0* mice after diet. (*D*–*G*) Densitometric analysis of plasma ApoB48 (*D*), ApoB100 (*E*), ApoE (*F*), and ApoA1 (*G*) immunoblots of fasted, aged *CFH*~ND, and ~HFC mice ($n = 8$–12). ApoB48 levels were increased in both aged *CFH*~HFC murine lines after HFC diet but no difference was observed between genotypes. ApoB100 was significantly higher in aged *CFH-Y/0*~HFC mice compared with aged *CFH-Y/0*~ND but was unchanged in *CFH-H/H* mice on ND or HFC diet. ApoE increased in both aged *CFH* mice lines on HFC diet compared with ND fed controls but aged *CFH-Y/0*~HFC mice had higher levels of ApoE than *CFH-H/H*~HFC mice. ApoA1 was unchanged in both genotypes after HFC diet. $^{*}P < 0.05$, $^{**}P < 0.01$, and $^{***}P < 0.001$ post hoc Tukey, respectively, following a significant genotype by diet interaction by ANOVA. Data are presented as mean ± SEM (*A*–*C*) and mean ± SD (*D*–*G*).

its potentially damaging effects (29). However, it is also possible that the H402 polymorphism could be impinging on an important function of intracellular CFH, as intracellular complement plays critical roles in cell survival, differentiation, and metabolism (62). Intracellular CFH can enhance cathepsin L-mediated cleavage of C3 and form complexes with nucleosomes in apoptotic cells to allow for efficient clearance of apoptotic cell debris (63) but whether this function of CFH is impaired by the Y402H polymorphism remains unknown. The *CFH-H/H*~HFC model of AMD supports the roles of these and other binding changes, contributing to the pathogenic mechanism responsible for the phenotype observed in these mice.

The differential binding of the H402 CFH variant to biomolecules may have a significant effect on lipid metabolism, as indicated by the differences in plasma lipoproteins and eyecup apolipoproteins between aged *CFH* mice on HFC diet. This is further supported by the overlap of biomolecules that lipoproteins and CFH can interact with. Specifically, lipoproteins bind heparan sulfates (64), harbor MDA epitopes when oxidized (65, 66), and carry thrombospondin-1 (67), which are all molecules that CFH can also interact with and that have been shown to be affected by the Y402H polymorphism (28, 29, 52). Thus, because the H402 polymorphism impacts the ability of CFH to bind to these biomolecules, it is reasonable to hypothesize that the changes observed in the lipoproteins and apolipoproteins in both the plasma and in the RPE/BrM/choroid lysates are due to the impaired binding of the CFH H402 variant to biomolecules. We found plasma LDL-cholesterol levels and its apolipoprotein markers ApoB100 and E are increased more in aged *CFH-Y/0*~HFC mice compared with aged *CFH-H/H*~HFC mice. The lower increase in plasma LDL in aged *CFH-H/H*~HFC mice is most likely due to a difference in clearance or retention, but not synthesis of LDL because LDL originates from VLDL remnants and plasma VLDL levels were unchanged between aged *CFH*~HFC mice. LDL can migrate through BrM and interact with LDL receptor on RPE cells in mice and nonhuman primates (68–70). Based on

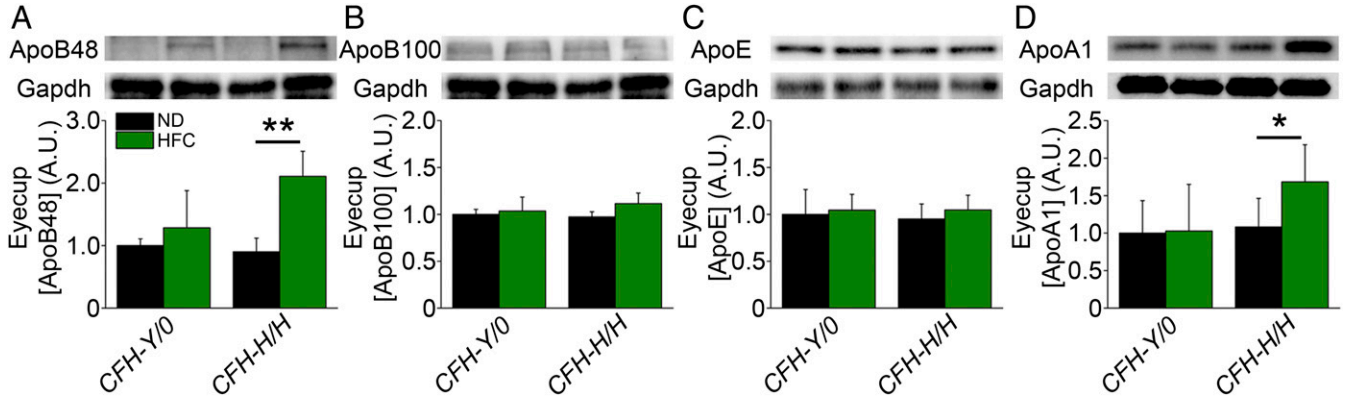

Fig. 5. Posterior eyecup apolipoprotein levels are *CFH* variant dependent. Densitometric analysis of ApoB48 (*A*), ApoB100 (*B*), ApoE (*C*), and ApoA1 (*D*) immunoblots of eyecup (RPE/BrM/choroid/sclera) lysates isolated from fasted and PBS-perfused, aged *CFH*~ND and ~HFC mice ($n = 4$–7). ApoB48 levels were higher in HFC-fed mice, but only the difference reached statistical significance in the *CFH-H/H* genotype. ApoB100 and ApoE were unchanged after HFC diet in both genotypes. ApoA1 levels were increased significantly in aged *CFH-H/H*~HFC compared with *CFH-H/H*~ND mice and were unchanged in aged *CFH-Y/0*~ND and ~HFC mice. $*P < 0.05$ and $**P < 0.01$ post hoc Tukey following a significant genotype by diet interaction by ANOVA for the densitometric arbitrary units, respectively. Data are presented as mean ± SD. Loading control (Gapdh) images in (*A*) and (*B*) are from the same blot because representative ApoB48 (*A*) and ApoB100 (*B*) images originate from the same set of samples on the same blot. Both ApoB isoforms are labeled on the same blot by the anti-ApoB antibody.

their increased BLamD accumulations, we hypothesized that ApoE- and ApoB100-containing LDL would be retained in the eyecups of aged *CFH-H/H*~HFC mice because CFH can compete with ApoE- and ApoB-containing lipoproteins for binding to GAGs in porcine and human BrM (31). However, only ApoB48 and ApoA1, but not ApoB100 or ApoE, are increased in the eyecups of aged *CFH-H/H*~HFC mice compared with age-matched *CFH-Y/0*~HFC mice. Because ApoE levels increased dramatically in the plasma and not in the eyecups of aged *CFH*~HFC mice, we posit that the increase of ApoB48 and ApoA1 in the eyecup lysates of aged *CFH-H/H*~HFC mice results from local RPE lipoprotein synthesis. Indeed, murine RPE expresses the molecular machinery required for lipoprotein secretion as well as *ApoB* and *ApoA1* transcripts (71–73). Although human RPE does not express the *APOBEC1* transcript and cannot synthesize the B48 isoform (74), ApoB48 can be detected in the media of palmitate-supplemented rat RPE cells and is believed to be expressed by mouse RPE (75, 76). It has been hypothesized that RPE-derived lipoproteins accumulate within BrM, become oxidized, and lead to the eventual formation of pathogenic drusen and AMD (77). The increase in ApoB48- and ApoA1-containing lipoproteins may explain the increase in deposit formation in aged *CFH-H/H* mice after HFC diet and could create a proinflammatory milieu in the sub-RPE that contributes to visual loss and RPE damage.

While we may infer the Y402H polymorphism impacts HFC-induced plasma LDL and RPE-derived lipoproteins, there are possible other functions of CFH affected by the H402 variant. Supporting this notion is our finding that BLamDs in aged *CFH-H/H*~ND mice are smaller than those observed in aged *CFH-Y/0*~ND mice. These data suggest that the H402 polymorphism impacts the lipoprotein accumulation and consequent deposit formation under normal diet and aging conditions. However, the composition of BLamDs under ambient conditions may not be largely comprised of lipoproteins in mice. Proteomic analyses of the BLamDs in the $Efemp^{R345W}$ knockin mouse model of Doyne's Honeycomb Retinal Dystrophy/Malattia Leventinese (DHRD/ML) revealed their composition is mostly extracellular matrix- and complement-related proteins but not apolipoproteins (78). We support these studies by finding no differences in the apolipoprotein eyecup content of aged *CFH-Y/0*~ND and *CFH-H/H*~ND mice. Interestingly, $Efemp^{R345W}$ knockin mice crossed to $C3^{-/-}$ mice do not develop deposit accumulations (78). This work, in conjunction with our current work, suggests complement may be driving the formation of deposits through multiple unrelated pathways. Future work is needed to identify these other pathways that are affected by the Y402H polymorphism and is beyond the scope of this study, as we do not observe a difference between the ERG responses and number of multinucleate RPE cells in ND-fed mice.

In conclusion, we present Y402 and H402 CFH variant differences in the response of posterior eye tissues and plasmas of aged mice after the consumption of an HFC diet. Our results suggest that the molecular differences explaining the phenotypes of aged *CFH-Y/0*~HFC and *CFH-H/H*~HFC mice are at the level of lipoprotein regulation and not complement activation. Thus, the role of the complement in AMD may lie at its function in lipid homeostasis and not at promoting inflammation. Targeting lipoprotein metabolism systemically using statins (79, 80) or locally using an apolipoprotein mimetic, such as an ApoA1 mimetic (81), may be viable therapeutic strategies for the treatment of AMD. Future studies should consider investigating the role of lipoproteins in the ocular phenotype of aged *CFH-H/H*~HFC mice using dietary and pharmacological interventions.

Materials and Methods

Animals and Diet. *CFH-Y/0* and *CFH-H/H* mice were generated and genotyped as described previously (42). No mice used in this study have the *rd8* mutation (82). Old (88–98 wk) and young adult (28–32 wk) *CFH-Y/0* and *CFH-H/H* mice were continued on a ND (Isopurina 5001; Prolab) or switched to an HFC diet (TD 88051; Envigo) for 8 wk. All mice were housed conventionally on a middle rack in the same mouse facility under ambient light conditions to control for environmental factors and microbiome fluctuations. Mice were maintained in accordance with the Institutional Animal Care and Use Committee at Duke University. The number of mice used for each experiment is provided in the figure legends.

Electroretinography. ERG was performed on mice following 4 h of dark adaption. Pupils were dilated with 0.5% tropicamide and 1.25% phenylephrine then mice were anesthetized with a combined mixture of ketamine (100 mg/kg) and xylazine (10 mg/kg). Scotopic ERGs were recorded using an Espion E2 system (Diagnosys), at increasing flash intensities, as described previously (83). Flash responses were smoothed using a low-pass noise-filtering script before analysis. The amplitude heights of the A-wave and B-wave for each ERG flash response were calculated and fitted using a previously published equation (83) in OriginPro 9.0 (OriginLab), as previously described (31, 42, 44, 47). Bmax1 and Bmax2 values were calculated as described (31).

RPE Flat Mounts. Eyes were enucleated following perfusion of the mouse with phosphate buffer solution (PBS). The anterior segment and retina were promptly removed, and the remaining RPE/choroid/sclera was fixed overnight

in methanol. RPE flat mounts were labeled with the rabbit antibody against ZO-1 (1:100, Invitrogen #40–2200) and nuclear stain Hoechst 33342 (1:500; Invitrogen), as previously described (31, 44, 47). Confocal images of the north, east, south, and west quadrants around the optic nerve were captured on an Eclipse C1 microscope (Nikon). Morphometric analysis was performed by a masked grader that counted the number of multinucleate RPE cells with three or more nuclei from each central quadrant.

Electron Microscopy. Eyes were enucleated following PBS and 2% glutaraldehyde/2% paraformaldehyde perfusion of the mouse and then fixed overnight in 2% glutaraldehyde/2% paraformaldehyde. Eyes were processed using routine methods previously described (42). Ultrathin sections of 60–80 nm were sectioned, mounted onto 400-mesh thin-bar copper grids (T400-Cu; Electron Microscopy Sciences), and stained with Sato's lead. Sections were imaged using a Tecnai G2 electron microscope. Images of the RPE/BrM were taken at each intersection of the tissue section with the copper grid and the largest BLamD within the EM image was measured using ImageJ software (NIH), as previously described (42). Approximately 62 ± 8 images per mouse were collected and scored for this study. Cumulative frequencies of the prevalence of deposit heights was determined to illustrate the distribution of deposit heights within each experimental group. Deposit height averages for each mouse were calculated for statistical comparisons between each experimental group.

RNA Isolation and RT-PCR of *CFH* Tissues. RNA from individual eyecups (RPE/choroid/sclera) was extracted using an RNeasy lipid tissue mini kit (Qiagen) according to the manufacturer's instructions. RNA concentrations were determined using the Nanodrop 2000 UV-Vis Spectrophotometer (Thermo Scientific). Expression of human *CFH* and mouse *C3* was examined in triplicate reactions using 12.5 ng cDNA from each eyecup RNA sample consisting of 200 nmol/L each primer and 12.5 μL iQTM SYBR Green Supermix (Bio-Rad) in 25 μL total volume. Primer sequences used in this study are *huCFH-F-GCTTTGAAAATGCCATACCC*, *huCFH-R-GGCCCACATTTTCCTGTAGA*, *mC3-F-GCGTCTCCATCAAGATTCCAGCCA*, *mC3-R-GCTACAGTCCCCAAAGTGTT*, *mRlpl0-F-GGACCCGAGAAGACCTCCTT*, and *mRlpl0-R-GCACATCACTCA-GAATTTCAATGG*. RT-PCR reactions were run in the CFX96 system (Bio-Rad) at 95 °C for 3 min, followed by 40 cycles at 95 °C for 10 s and 60 °C for 20 s, then 72 °C for 15 s. Relative mRNA expression was normalized to the endogenous reference murine gene ribosomal protein lateral stalk subunit P0 (*Rlpl0*) using the quantitative $2^{-\Delta\Delta C}$T method (84).

Western Blots of *CFH* Tissues. Mice were fasted for 5 h from 10:00 AM to 3:00 PM and bled via the submandibular vein into EDTA tubes (BD Microtainer; BD). Blood was spun for 15 min at 1,200 g and plasma was collected. Mice were then killed with CO_2 and promptly perfused with 1× PBS to remove blood contamination from the eyes. Eyes were enucleated, and the anterior segment and retina were removed from the posterior eyecup (RPE/choroid/sclera) and stored at −80 °C. Eyecup lysates were made by manually homogenizing tissues with a handheld micro grinder (Argos Technologies) in 80 μL of RIPA buffer (Thermo Scientific) containing protease inhibitor (Roche) and quantified using the Pierce BCA Protein Assay Kit (Thermo Scientific). Plasma samples were diluted in 10% XT Sample buffer (Bio-Rad) and equal dilution volumes were aliquoted and equal eyecup protein concentrations were pipetted to sample buffer before running on 10% Bis·Tris Criterion XT gels (Bio-Rad) in Mops buffer (Bio-Rad) under nonreducing conditions and transferred to nitrocellulose membranes (Bio-Rad). For the plasma iC3b Westerns, XT reducing agent (Bio-Rad) was added to each sample and followed by incubation at 105 °C for 7 min. Membranes were probed for CFH (goat anti-CFH, A312; Quidel), C3 (rabbit anti-human C3d, A0063; Dako), FB (goat anti-FB; Kent Laboratories), ApoE (goat anti-ApoE, 178479; Calbiochem), ApoB (goat anti-ApoB, AB742), and ApoA1 (goat anti-ApoA, 11A-G2b; Academy Bio-Medical) overnight at 4 °C. Blots were washed with TBST buffer and incubated with either peroxidase-conjugated anti-goat or anti-rabbit IgG (Jackson ImmunoResearch), depending on the source of the primary antibody. Blots were washed again with TBST and incubated with ECL Plus reagent (Thermo Scientific). Blots were imaged using a ChemiDoc Imaging System (Bio-Rad) and analyzed using ImageJ software (NIH). For loading controls, blots containing plasma samples were reprobed for albumin (rabbit anti-albumin, ab31657-1; Abcam) and blots containing eyecup lysates were probed for Gapdh (rabbit anti-Gapdh, 2118; Cell Signaling).

Cholesterol Measurement. Plasma cholesterol and lipoprotein-associated cholesterol were measured with the Amplex Red Cholesterol Assay Kit (ThermoFisher Scientific) using the manufacturer's guidelines. Fluorescence was measured using a Spectramax M5 plate reader (Molecular Devices).

Lipoprotein Fractionation. Thirty microliters of plasma from each *CFH*∼ND and *CFH*∼HFC mouse was fractionated on an FPLC system (AKTA Pure; GE Healthcare) with a Superose 6HR 10/30 column (GE Healthcare) into 500-μL fractions. Cholesterol was measured in fractions 13 through 31.

Statistical Analysis. ANOVA statistical analysis with post hoc Tukey test or student's two-sided *t* test analyses were used to calculate statistical significance. Detailed descriptions of the comparisons are described in the figure legends. Statistical analyses were performed in JMP Pro-9 software.

ACKNOWLEDGMENTS. The authors thank Ying Hao for her expert technical assistance with electron microscopy; and Dan Stamer, Scott Cousins, Michael Hauser, Daniel Saban, and Yuan Zhuang for their intellectual feedback and advice. This work was supported by National Eye Institute funding Grants R01 EY026161 (to C.B.R.) and P30 EY005722 (to Duke Eye Center); a Research to Prevent Blindness/International Retinal Research Foundation Catalyst award for Innovative Research Approaches for AMD (to C.B.R.); an unrestricted grant from Research to Prevent Blindness (to the Duke Eye Center); a Macular Degeneration Research Award grant from the BrightFocus Foundation (to M.K.); and a Fighting Blindness Individual Investigator award (to C.B.R.).

1. Wong WL, et al. (2014) Global prevalence of age-related macular degeneration and disease burden projection for 2020 and 2040: A systematic review and meta-analysis. *Lancet Glob Health* 2:e106–e116.
2. Chew EY, et al.; Age-Related Eye Disease Study Research Group (2014) Ten-year follow-up of age-related macular degeneration in the age-related eye disease study: AREDS report no. 36. *JAMA Ophthalmol* 132:272–277.
3. Fritsche LG, et al. (2014) Age-related macular degeneration: Genetics and biology coming together. *Annu Rev Genomics Hum Genet* 15:151–171.
4. Lambert NG, et al. (2016) Risk factors and biomarkers of age-related macular degeneration. *Prog Retin Eye Res* 54:64–102.
5. Seddon JM, et al. (2013) Rare variants in CFI, C3 and C9 are associated with high risk of advanced age-related macular degeneration. *Nat Genet* 45: 1366–1370.
6. Hageman GS, et al. (2005) A common haplotype in the complement regulatory gene factor H (HF1/CFH) predisposes individuals to age-related macular degeneration. *Proc Natl Acad Sci USA* 102:7227–7232.
7. Klein RJ, et al. (2005) Complement factor H polymorphism in age-related macular degeneration. *Science* 308:385–389.
8. Edwards AO, et al. (2005) Complement factor H polymorphism and age-related macular degeneration. *Science* 308:421–424.
9. Haines JL, et al. (2005) Complement factor H variant increases the risk of age-related macular degeneration. *Science* 308:419–421.
10. Raychaudhuri S, et al. (2011) A rare penetrant mutation in CFH confers high risk of age-related macular degeneration. *Nat Genet* 43:1232–1236.
11. Maller JB, et al. (2007) Variation in complement factor 3 is associated with risk of age-related macular degeneration. *Nat Genet* 39:1200–1201.
12. Gold B, et al.; AMD Genetics Clinical Study Group (2006) Variation in factor B (BF) and complement component 2 (C2) genes is associated with age-related macular degeneration. *Nat Genet* 38:458–462.
13. Helgason H, et al. (2013) A rare nonsynonymous sequence variant in C3 is associated with high risk of age-related macular degeneration. *Nat Genet* 45:1371–1374.
14. Sarma JV, Ward PA (2011) The complement system. *Cell Tissue Res* 343:227–235.
15. Hajishengallis G, Reis ES, Mastellos DC, Ricklin D, Lambris JD (2017) Novel mechanisms and functions of complement. *Nat Immunol* 18:1288–1298.
16. Yaspan BL, et al.; MAHALO Study Investigators (2017) Targeting factor D of the alternative complement pathway reduces geographic atrophy progression secondary to age-related macular degeneration. *Sci Transl Med* 9:eaaf1443.
17. DiScipio RG (1992) Ultrastructures and interactions of complement factors H and I. *J Immunol* 149:2592–2599.
18. Sharma AK, Pangburn MK (1996) Identification of three physically and functionally distinct binding sites for C3b in human complement factor H by deletion mutagenesis. *Proc Natl Acad Sci USA* 93:10996–11001.
19. Kelly U, et al. (2010) Heparan sulfate, including that in Bruch's membrane, inhibits the complement alternative pathway: Implications for age-related macular degeneration. *J Immunol* 185:5486–5494.
20. Rodríguez de Córdoba S, Esparza-Gordillo J, Goicoechea de Jorge E, Lopez-Trascasa M, Sánchez-Corral P (2004) The human complement factor H: Functional roles, genetic variations and disease associations. *Mol Immunol* 41:355–367.
21. Skerka C, et al. (2007) Defective complement control of factor H (Y402H) and FHL-1 in age-related macular degeneration. *Mol Immunol* 44:3398–3406.
22. Zipfel PF, Skerka C (2009) Complement regulators and inhibitory proteins. *Nat Rev Immunol* 9:729–740.

23. Fearon DT (1978) Regulation by membrane sialic acid of beta1H-dependent decay-dissociation of amplification C3 convertase of the alternative complement pathway. *Proc Natl Acad Sci USA* 75:1971–1975.
24. Mold C, Kingzette M, Gewurz H (1984) C-reactive protein inhibits pneumococcal activation of the alternative pathway by increasing the interaction between factor H and C3b. *J Immunol* 133:882–885.
25. Ormsby RJ, et al. (2008) Functional and structural implications of the complement factor H Y402H polymorphism associated with age-related macular degeneration. *Invest Ophthalmol Vis Sci* 49:1763–1770.
26. Yu J, et al. (2007) Biochemical analysis of a common human polymorphism associated with age-related macular degeneration. *Biochemistry* 46:8451–8461.
27. Molins B, et al. (2016) Complement factor H binding of monomeric C-reactive protein downregulates proinflammatory activity and is impaired with at risk polymorphic CFH variants. *Sci Rep* 6:22889.
28. Clark SJ, et al. (2010) Impaired binding of the age-related macular degeneration-associated complement factor H 402H allotype to Bruch's membrane in human retina. *J Biol Chem* 285:30192–30202.
29. Weismann D, et al. (2011) Complement factor H binds malondialdehyde epitopes and protects from oxidative stress. *Nature* 478:76–81.
30. Shaw PX, et al. (2012) Complement factor H genotypes impact risk of age-related macular degeneration by interaction with oxidized phospholipids. *Proc Natl Acad Sci USA* 109:13757–13762.
31. Toomey CB, Kelly U, Saban DR, Bowes Rickman C (2015) Regulation of age-related macular degeneration-like pathology by complement factor H. *Proc Natl Acad Sci USA* 112:E3040–E3049.
32. Pickering MC, et al. (2002) Uncontrolled C3 activation causes membranoproliferative glomerulonephritis in mice deficient in complement factor H. *Nat Genet* 31:424–428.
33. Toomey CB, Johnson LV, Bowes Rickman C (2018) Complement factor H in AMD: Bridging genetic associations and pathobiology. *Prog Retin Eye Res* 62:38–57.
34. Vergnes L, Phan J, Strauss M, Tafuri S, Reue K (2003) Cholesterol and cholate components of an atherogenic diet induce distinct stages of hepatic inflammatory gene expression. *J Biol Chem* 278:42774–42784.
35. Colijn JM, et al. (October 10, 2018) Increased high density lipoprotein-levels associated with age-related macular degeneration. Evidence from the EYE-RISK and E3 Consortia. *Ophthalmology*, 10.1016/j.ophtha.2018.09.045.
36. Fan Q, et al. (2017) HDL-cholesterol levels and risk of age-related macular degeneration: A multiethnic genetic study using Mendelian randomization. *Int J Epidemiol* 46:1891–1902.
37. Cheung CMG, et al. (2017) Plasma lipoprotein subfraction concentrations are associated with lipid metabolism and age-related macular degeneration. *J Lipid Res* 58: 1785–1796.
38. Burgess S, Davey Smith G (2017) Mendelian randomization implicates high-density lipoprotein cholesterol-associated mechanisms in etiology of age-related macular degeneration. *Ophthalmology* 124:1165–1174.
39. Yip JL, et al. (2015) Cross sectional and longitudinal associations between cardiovascular risk factors and age related macular degeneration in the EPIC-Norfolk eye study. *PLoS One* 10:e0132565.
40. Zee RY, Diehl KA, Ridker PM (2006) Complement factor H Y402H gene polymorphism, C-reactive protein, and risk of incident myocardial infarction, ischaemic stroke, and venous thromboembolism: A nested case-control study. *Atherosclerosis* 187:332–335.
41. Sofat R, et al. (2010) Genetic variation in complement factor H and risk of coronary heart disease: Eight new studies and a meta-analysis of around 48,000 individuals. *Atherosclerosis* 213:184–190.
42. Ding JD, et al. (2015) Expression of human complement factor H prevents age-related macular degeneration-like retina damage and kidney abnormalities in aged Cfh knockout mice. *Am J Pathol* 185:29–42.
43. Mandal MN, Ayyagari R (2006) Complement factor H: Spatial and temporal expression and localization in the eye. *Invest Ophthalmol Vis Sci* 47:4091–4097.
44. Ding JD, et al. (2011) Anti-amyloid therapy protects against retinal pigmented epithelium damage and vision loss in a model of age-related macular degeneration. *Proc Natl Acad Sci USA* 108:E279–E287.
45. Malek G, et al. (2005) Apolipoprotein E allele-dependent pathogenesis: A model for age-related retinal degeneration. *Proc Natl Acad Sci USA* 102:11900–11905.
46. Owsley C, et al. (2016) Delayed rod-mediated dark adaptation is a functional biomarker for incident early age-related macular degeneration. *Ophthalmology* 123: 344–351.
47. Toomey CB, et al. (2018) Effect of anti-C5a therapy in a murine model of early/intermediate dry age-related macular degeneration. *Invest Ophthalmol Vis Sci* 59: 662–673.
48. Chen M, et al. (2016) Retinal pigment epithelial cell multinucleation in the aging eye—A mechanism to repair damage and maintain homoeostasis. *Aging Cell* 15:436–445.
49. Curcio CA (2018) Soft drusen in age-related macular degeneration: Biology and targeting via the oil spill strategies. *Invest Ophthalmol Vis Sci* 59:AMD160–AMD181.
50. Aredo B, et al. (2015) A chimeric *Cfh* transgene leads to increased retinal oxidative stress, inflammation, and accumulation of activated subretinal microglia in mice. *Invest Ophthalmol Vis Sci* 56:3427–3440.
51. Ufret-Vincenty RL, et al. (2010) Transgenic mice expressing variants of complement factor H develop AMD-like retinal findings. *Invest Ophthalmol Vis Sci* 51:5878–5887.
52. Calippe B, et al. (2017) Complement factor H inhibits CD47-mediated resolution of inflammation. *Immunity* 46:261–272.
53. Anderson DH, et al. (2010) The pivotal role of the complement system in aging and age-related macular degeneration: Hypothesis re-visited. *Prog Retin Eye Res* 29: 95–112.
54. Scholl HP, et al. (2008) Systemic complement activation in age-related macular degeneration. *PLoS One* 3:e2593.
55. Lechner J, et al. (2016) Higher plasma levels of complement C3a, C4a and C5a increase the risk of subretinal fibrosis in neovascular age-related macular degeneration: Complement activation in AMD. *Immun Ageing* 13:4.
56. Silva AS, et al. (2012) Plasma levels of complement proteins from the alternative pathway in patients with age-related macular degeneration are independent of Complement Factor H Tyr(4)(0)(2)His polymorphism. *Mol Vis* 18:2288–2299.
57. Reynolds R, et al. (2009) Plasma complement components and activation fragments: Associations with age-related macular degeneration genotypes and phenotypes. *Invest Ophthalmol Vis Sci* 50:5818–5827.
58. Crabb JW, et al. (2002) Drusen proteome analysis: An approach to the etiology of age-related macular degeneration. *Proc Natl Acad Sci USA* 99:14682–14687.
59. Anderson DH, Mullins RF, Hageman GS, Johnson LV (2002) A role for local inflammation in the formation of drusen in the aging eye. *Am J Ophthalmol* 134:411–431.
60. Johnson LV, Leitner WP, Staples MK, Anderson DH (2001) Complement activation and inflammatory processes in Drusen formation and age related macular degeneration. *Exp Eye Res* 73:887–896.
61. Yehoshua Z, et al. (2014) Systemic complement inhibition with eculizumab for geographic atrophy in age-related macular degeneration: The COMPLETE study. *Ophthalmology* 121:693–701.
62. Reichhardt MP, Meri S (2018) Intracellular complement activation-An alarm raising mechanism? *Semin Immunol* 38:54–62.
63. Martin M, et al. (2016) Factor H uptake regulates intracellular C3 activation during apoptosis and decreases the inflammatory potential of nucleosomes. *Cell Death Differ* 23:903–911.
64. Ji ZS, Dichek HL, Miranda RD, Mahley RW (1997) Heparan sulfate proteoglycans participate in hepatic lipaseand apolipoprotein E-mediated binding and uptake of plasma lipoproteins, including high density lipoproteins. *J Biol Chem* 272:31285–31292.
65. Parthasarathy S, Raghavamenon A, Garelnabi MO, Santanam N (2010) Oxidized low-density lipoprotein. *Methods Mol Biol* 610:403–417.
66. Guertin F, Brunet S, Gavino V, Tuchweber B, Levy E (1994) Malondialdehyde-modified high-density lipoprotein cholesterol: Plasma removal, tissue distribution and biliary sterol secretion in rats. *Biochim Biophys Acta* 1214:137–142.
67. Mangé A, et al. (2012) HDL proteome in hemodialysis patients: A quantitative nanoflow liquid chromatography-tandem mass spectrometry approach. *PLoS One* 7: e34107.
68. Tserentsoodol N, et al. (2006) Uptake of cholesterol by the retina occurs primarily via a low density lipoprotein receptor-mediated process. *Mol Vis* 12:1306–1318.
69. Gordiyenko N, et al. (2004) RPE cells internalize low-density lipoprotein (LDL) and oxidized LDL (oxLDL) in large quantities in vitro and in vivo. *Invest Ophthalmol Vis Sci* 45:2822–2829.
70. Elner VM (2002) Retinal pigment epithelial acid lipase activity and lipoprotein receptors: Effects of dietary omega-3 fatty acids. *Trans Am Ophthalmol Soc* 100: 301–338.
71. Fujihara M, Bartels E, Nielsen LB, Handa JT (2009) A human apoB100 transgenic mouse expresses human apoB100 in the RPE and develops features of early AMD. *Exp Eye Res* 88:1115–1123.
72. Zheng W, Mast N, Saadane A, Pikuleva IA (2015) Pathways of cholesterol homeostasis in mouse retina responsive to dietary and pharmacologic treatments. *J Lipid Res* 56: 81–97.
73. Zheng W, et al. (2012) Spatial distribution of the pathways of cholesterol homeostasis in human retina. *PLoS One* 7:e37926.
74. Li CM, et al. (2005) Retina expresses microsomal triglyceride transfer protein: Implications for age-related maculopathy. *J Lipid Res* 46:628–640.
75. Wang L, et al. (2009) Lipoprotein particles of intraocular origin in human Bruch membrane: An unusual lipid profile. *Invest Ophthalmol Vis Sci* 50:870–877.
76. Handa JT, Cano M, Wang L, Datta S, Liu T (2017) Lipids, oxidized lipids, oxidation-specific epitopes, and Age-related Macular Degeneration. *Biochim Biophys Acta Mol Cell Biol Lipids* 1862:430–440.
77. Curcio CA, Johnson M, Rudolf M, Huang JD (2011) The oil spill in ageing Bruch membrane. *Br J Ophthalmol* 95:1638–1645.
78. Garland DL, et al. (2014) Mouse genetics and proteomic analyses demonstrate a critical role for complement in a model of DHRD/ML, an inherited macular degeneration. *Hum Mol Genet* 23:52–68.
79. Vavvas DG, et al. (2016) Regression of some high-risk features of age-related macular degeneration (AMD) in patients receiving intensive statin treatment. *EBioMedicine* 5: 198–203.
80. Guymer RH, et al. (2013) Proof of concept, randomized, placebo-controlled study of the effect of simvastatin on the course of age-related macular degeneration. *PLoS One* 8:e83759.
81. Rudolf M, et al. (2018) ApoA-I mimetic peptide 4F reduces age-related lipid deposition in murine Bruch's membrane and causes its structural remodeling. *Curr Eye Res* 43:135–146.
82. Mattapallil MJ, et al. (2012) The Rd8 mutation of the Crb1 gene is present in vendor lines of C57BL/6N mice and embryonic stem cells, and confounds ocular induced mutant phenotypes. *Invest Ophthalmol Vis Sci* 53:2921–2927.
83. Herrmann R, et al. (2010) Phosducin regulates transmission at the photoreceptor-to-ON-bipolar cell synapse. *J Neurosci* 30:3239–3253.
84. Livak KJ, Schmittgen TD (2001) Analysis of relative gene expression data using real-time quantitative PCR and the 2(-Delta Delta C(T)) Method. *Methods* 25:402–408.